Journal of Cell Science 111, 2337-2351 (1998)
Printed in Great Britain © The Company of Biologists Limited 1998
JCS3779



# Aspects of three-dimensional chromosome reorganization during the onset of human male meiotic prophase

**H. Scherthan[1,2,*], R. Eils[3,**], E. Trelles-Sticken[1], S. Dietzel[4,‡], T. Cremer[5], H. Walt[6] and A. Jauch[4]**

[1]Abt. Humanbiologie and [2]Abt. Zellbiologie, der Universität, Postf. 3049, D-67653 Kaiserslautern, Germany
[3]Interdisziplinäres Zentrum für Wissenschaftliches Rechnen, INF 368, D-69120 Heidelberg, Germany
[4]Inst. für Humangenetik and Anthropologie, INF 328, D-69120 Heidelberg, Germany
[5]Inst. für Anthropologie und Humangenetik, L-M-U München, R.-Wagner Str.10/I, D-80333 München, Germany
[6]Dept. für Frauenheilkunde, Universitätsspital Zürich, CH-8091 Zürich, Switzerland
*Author for correspondence (e-mail: scherth@rhrk.uni-kl.de)
‡Present address: Dept of Cell and Structural Biology, University of Illinois at Urbana Champaign, USA
**The first two authors contributed equally to this study

*Accepted 2 June; published on WWW 30 July 1998*

## SUMMARY

**The three-dimensional morphology and distribution of human chromosomes 3 were studied in nuclei of spermatogonia and spermatocytes I from formaldehyde-fixed human testis sections. Chromosome arms, pericentromeres and telomeric regions were painted by a three-color, five-probe fluorescence in situ hybridization protocol. Light optical serial sections of premeiotic and meiotic nuclei obtained by confocal laser scanning microscopy revealed that premeiotic chromosomes 3 are separate from each other and occupy variably shaped territories, which are sectored in distinct 3 p- and q-arm domains. Three-dimensional reconstructions of the painted chromosome domains by a Voronoi tessellation approach showed that mean chromosome volumes did not differ significantly among the premeiotic and meiotic stages investigated. A significant increase in surface area and reduction of dimensionless 'roundness factor' estimates of arm domains indicated that the restructuring of spatially separate chromosome territories initiates during preleptotene. Telomeric regions, which in meiotic stem cells located predominantly in arm-domain chromatin, showed a redistribution towards the domain surface during this stage. At leptotene homologues were generally misaligned and displayed intimate intermingling of non-homologous chromatin. Pairing initiated at the ends of bent zygotene chromosomes, which displayed a complex surface structure with discernible sister chromatids. The results indicate that, in mammals, homology search is executed during leptotene, after remodeling of chromosome territories.**

Key words: Meiosis, Fluorescence in situ hybridization, FISH, Human, Spermatogenesis, Homology search, Chromosome pairing

## INTRODUCTION

Meiosis is a specialized cell division that reduces the diploid chromosome number to haploid, thereby compensating for the genome doubling that occurs at fertilization. Prior to their segregation at metaphase I, homologous chromosomes recognize, align and initiate synapsis. This process is coordinated during an extended prophase (for reviews see von Wettstein et al., 1984; Loidl, 1990). At leptotene an axial core (element) assembles along replicated sister chromatids. At zygotene transverse filaments start to interconnect axial cores (now designated lateral elements), forming the well-known tripartite structure of the synaptonemal complex (SC), which tightly connects all homologues at pachytene (Schmekel and Daneholt, 1995; Heyting 1996). Recent genetical, biochemical and cytological analyses of meiosis indicate that a meiotic homology search process operates independently of recombination and synapsis (for reviews see Hawley and Arbel, 1993; Roeder, 1995; Kleckner, 1996). In a few organisms, chromosome search and pairing at meiotic prophase profit from a premeiotic chromosome association (Wandall and Svendsen 1985; Hiraoka et al., 1993; Scherthan et al., 1994; Weiner and Kleckner, 1994; Schwarzacher, 1997), while in most organisms this seems not to be the case (von Wettstein et al., 1984; Dawe et al., 1994; Armstrong et al., 1994; Scherthan et al., 1996; Bass et al., 1997).

Based on the omnipresence of telomere clustering during leptotene/zygotene of nearly all sexually reproducing organisms (for a review see Dernburg et al., 1995), it has been proposed that telomere movements and clustering facilitate homology search and alignment, and that this process operates during leptotene (see e.g. Moses, 1968; Scherthan et al., 1996). However, studies which identify the overall morphology and orientation of three-dimensionally preserved chromatin of homologous chromosomes prior to and during the onset of meiotic prophase are scarce. In the mouse, an extremely short

leptotene prophase stage (Oud and Reutlinger, 1981; Dietrich and de Boer, 1983) and the absence of appropriately performing whole chromosome paint probes for interphase fluorescence in situ hybridization (FISH), have so far prevented such an analysis.

In the present investigation we have exploited the extended duration of human meiotic prophase (Adler, 1996) to perform a high resolution study on the three-dimensional distribution and organization of chromosomes and subdomains in meiotic stem cells, and their reorganization and spatial redistribution during meiotic prophase up to pachytene. To this end, chromosome arm chromatin, the centromeric and both telomeric regions of human metacentric chromosomes 3, were distinctly illuminated by a three-color, five-probe FISH-labeling scheme. FISH was performed on nuclei structurally preserved from human paraffin-embedded testis sections (Scherthan and Cremer, 1994), and disclosed that the restructuring of chromosome territories commenced during preleptotene. At leptotene spatially separate homologues underwent a dramatic reorientation. Confocal laser scanning microscopy in conjunction with quantitative image analysis and three-dimensional reconstruction (Eils et al., 1996) has revealed the first quantitative description of the remodeling of the three-dimensional structure of human chromosome 3 territories in spermatogonia and spermatocyte I nuclei up to pachytene.

## MATERIALS AND METHODS

### DNA probes and labeling

Chromosome arm-specific microdissection libraries to chromosomes 3 (Guan et al., 1996) were kindly provided by J. Trent, NIH, USA. A repetitive, chromosome 3 centromeric α-satellite DNA probe (pα3.5; Waye and Willard, 1989) was used to label chromosome 3 pericentromeric regions. A YAC clone for 3pter (TYAC148; 300 kbp) and a 3qter YAC (TYAC162, 250 kbp) (Vocero-Akbani et al., 1996) were used to stain both terminal regions of chromosomes 3.

DNA of the microdissection libraries was amplified by DOP-PCR as published previously (Guan et al., 1996). DNA probes were labeled with biotin-14-dATP (Life Technologies) or digoxigenin-11-dUTP (Boehringer-Mannheim) using a nick translation kit, according to the instructions of the supplier (Life Technologies). The α-satellite DNA probe was labeled directly by nick translation with FITC-dUTP (Boehringer-Mannheim).

### Tissue origin and processing

Human testis tissue was obtained by biopsy and fixed for 4 hours in phosphate-buffered formaldehyde (4% in PBS). Thereafter, tissue was embedded in paraffin, 12 μm sections were cut from paraffin blocks and stuck to 3-aminotriethoxy-propylsilane (Merck) -coated slides (see Scherthan and Cremer, 1994).

### In situ hybridization to tissue sections and probe detection

Pretreatment as well as fluorescence in situ hybridization to paraffin tissue sections was performed as described in detail by Scherthan and Cremer (1994). In situ hybridization was carried out for 72 hours. After post-hybridization washes, biotinylated probe molecules were detected by incubating the hybridized slides with avidin-Cy3 (Sigma). Digoxigenin (dig)-labeled hybrid molecules were detected using a primary anti-dig mouse monoclonal antibody (Boehringer-Mannheim) followed by a subsequent incubation with a Cy5-conjugated rabbit anti-mouse antibody (Jackson).

### Light microscopic evaluation and image recording

Preparations were evaluated using a Zeiss Axioskop epifluorescence microscope equipped with single-band-pass filters for excitation of blue, green, red and far-red (Cy5) fluorescence (Chroma Technologies). Digital black-and-white images were recorded with a cooled CCD-camera (Hamamatsu) coupled to the ISIS fluorescence image analysis system (MetaSystems).

Light optical serial sectioning was performed using a Leica confocal laser scanning microscope (Leica TCS 4D; Leica) equipped with a Plan Apo 63×/1.4 oil immersion lens. Using the appropriate lines of an Argon/Krypton laser (488 nm, 567 nm and 647 nm) for the visualization of FITC, Cy3 and Cy5, respectively, stacks of equidistant (0.25 μm) 8 bit grayscale images of 256×256 pixel size (25×25 μm) were recorded. Each line was scanned 8 times and averaged. Consecutive scans of each color were obtained before moving in an axial direction to avoid z-shifts introduced by the step motor. Depending on the height of the respective nucleus, each stack consisted of 20-42 images. Image stacks were transferred to a Silicon Graphics workstation (SGI Maximum Impact, CPU R10000, 200 MHz, 196 MB RAM) for further analysis.

### Three-dimensional reconstruction and morphological analysis of painted chromosome territories and centromeric regions

For a quantitative analysis of painted sub-chromosomal arm territories the three-dimensional (3-D) Voronoi approach was applied as described (Eils et al., 1995a; 1996). For this purpose the three-dimensional image volume, represented by the stack of light optical serial sections from a given cell nucleus, was iteratively tessellated into polyhedra. Each polyhedron represents a subvolume with voxels of similar gray value intensities. Chromosome territories were extracted as a set of connected polyhedra with similar mean intensity, i.e. the associated mean gray value of all voxels belonging to each polyhedron exceeded a common preset gray value threshold. After 3-D segmentation, chromosome territory volume (V), surface (S) and a roundness factor (RF) were computed. RF is defined as:

$$RF = 36\pi \frac{V^2}{S^3},$$

where $0<RF<1$. A roundness factor of 1 corresponds to a perfectly round and smooth shape of a sphere, whereas RF decreases with increasing surface roughness and/or elongation of three-dimensional shape.

Tessellation of the image stacks into polyhedra largely reduces the amount of data to be handled by the computer in order to visualize three-dimensional objects such as chromosome territories by ray tracing (Quien and Müller, 1992) and is particularly suited for calculating morphological parameters such as volume, surface and shape (see Eils et al., 1995a, 1996).

The Voronoi tessellation procedure was applied to each of the two image channels containing the chromosome 3 arm-domain signals of a given nucleus. The only required user interaction was the definition of a threshold for the segmentation of the arm territories. To avoid a user bias the arm territories were segmented over a reasonable threshold range as described previously (Eils et al., 1995a). It is an inherent feature of the Voronoi approach that volume, surface and shape variations over the threshold range are relatively small (±20% s.d.). For statistical analysis the morphological parameters were averaged over the whole threshold range and then exported into the software package Lotus®1-2-3.

To calculate the volume of the centromeric regions of chromosomes 3, the interactive image analysis package *showpos* was applied (K. Sätzler and R. Eils, unpublished data). This program allows a browse through the image stacks. Regions of interest can be marked by a mouse click and segmented from the background using an interactive thresholding approach. The output of *showpos* is a file

revealing both the volume and the geometrical gravity center of the interactively identified signals in subsequent images of a stack. Statistical analysis was performed thereafter using the Lotus®1-2-3 software package.

### Three-dimensional distance measurements

Distances between chromosome 3 arm domain surfaces and telomeric regions were computed as the shortest distance between the Voronoi-tessellated chromosome arm domain surface and the gravity center of the signal created by a telomeric probe (Eils et al., 1995b). Chromosome arms were segmented in the Voronoi diagram over a reasonable threshold range (see above). The gravity centers of the telomeric signals were obtained in a semi-automated way using the program *showpos* (see above). Distances obtained at each threshold level were averaged over the whole threshold range and exported into Lotus®1-2-3 for further analysis.

## RESULTS

We have investigated the reorientation and three-dimensional restructuring of subdomains of a pair of metacentric human chromosomes during progression of meiotic prophase. A five-probe, three-color FISH scheme was applied, which simultaneously illuminated chromosome 3 p- and q-arms, pericentromeres and both telomeric regions (Fig. 1) in structurally preserved spermatogenetic cells from paraffin-embedded testis tissue sections. Nuclei of meiotic stem cells (spermatogonia) and spermatocytes I at various meiotic prophase stages up to pachytene were analyzed by conventional fluorescence microscopy and by optical serial sectioning using a confocal laser scanning microscope.

In a given cross section of a human testis, tubule cells at various stages of differentiation can be discerned, since spermatocyte populations of the same degree of development are arranged on helices along the longitudinal course of seminiferous tubules (Schulze and Rehder, 1984). Spermatogonia were identified by their close apposition to the tubule membrane, while spermatocytes were remote from it and displayed a larger diameter and threadlike chromatin upon DAPI staining (Fig. 2). When applied, the FISH protocol (Scherthan et al., 1996) rendered strong hybridization signals with distinct borders in structurally preserved tissue section nuclei (Figs 3-5). Preleptotene spermatocytes were identified by the decondensed pericentromeric satellite DNA signal (Fig. 3), while the fiber-like morphology and the spatial relationship of homologous chromosome territories identified leptotene, zygotene and pachytene spermatocytes (see Figs 5, 9; compare also Scherthan et al., 1996). To minimize influences of technical variation on the data set, only nuclei from the same experiment and tissue section were optically serial sectioned. The confocal image stacks obtained were further investigated by quantitative mathematical analysis using the Voronoi tessellation algorithm. This analysis provides estimates of volume, surface area and roundness factor, the latter being a dimensionless measure for chromosome morphology (see Materials and Methods). Threshold levels for segmentation of three-dimensionally reconstructed chromosome arm domains were adjusted such that the arm domain signals were separated from surrounding background noise (generally 10-15% of signal values) and that the reconstructed chromosomes mirrored the details of signal distribution seen in the confocal gray value images (for details see Eils et al., 1996; compare also Figs 4 and 5). Values for volume, surface area and roundness factor were calculated for separate signals of homologous domains detected in spermatogonia, preleptotene and leptotene nuclei. In each zygotene nucleus there was at

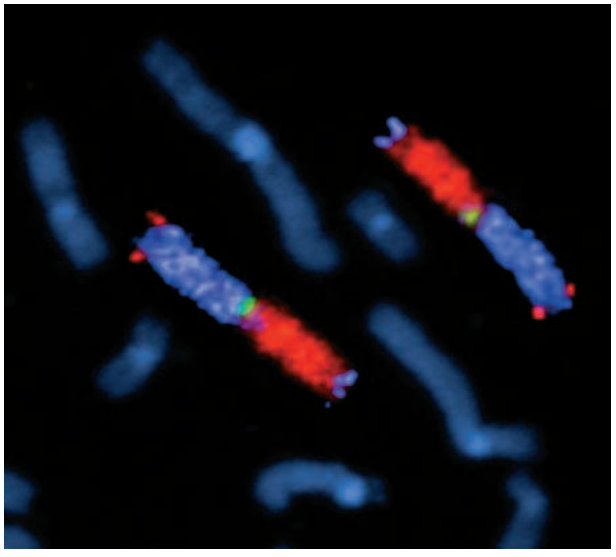

**Fig. 1.** Three-color, five-probe FISH of human metaphase chromosomes. Human chromosomes 3 were delineated such that the 3p telomere and 3q arms light up in red (Cy3), the 3q telomeres and the 3p arms light up in pink-blue (Cy5, false color), and the chromosome 3 centromeric regions in green (fluorescein). Digital epi-fluorescence microscopy of a DAPI-stained partial human metaphase spread.

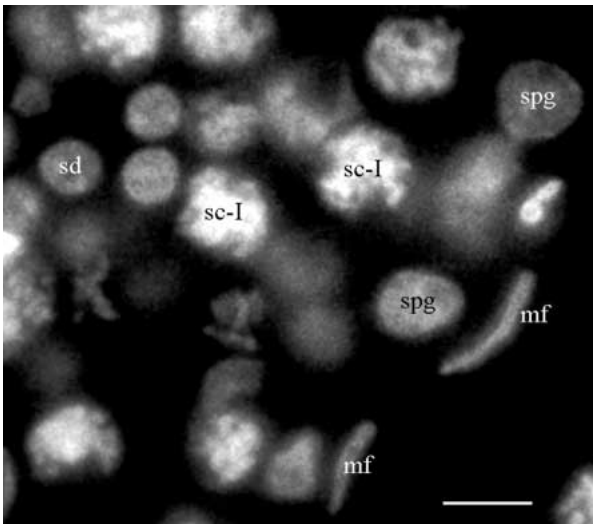


**Fig. 2.** Detail of a DAPI-stained human testis tubule after FISH. The periphery of the tubule is marked by the two oblong nuclei of myofibroblast cells (mf) which locate adjacent to the tubule membrane. Nuclei of spermatogonia (spg) are found in the vicinity of the mf-nuclei, while nuclei of pachytene spermatocytes (sc-I) display thread-like chromatin and are seen more remote from the spg- and the mf-nuclei. Nuclei of round spermatids (sd) are also seen. Conventional fluorescence microscopy. Bar, 10 μm.

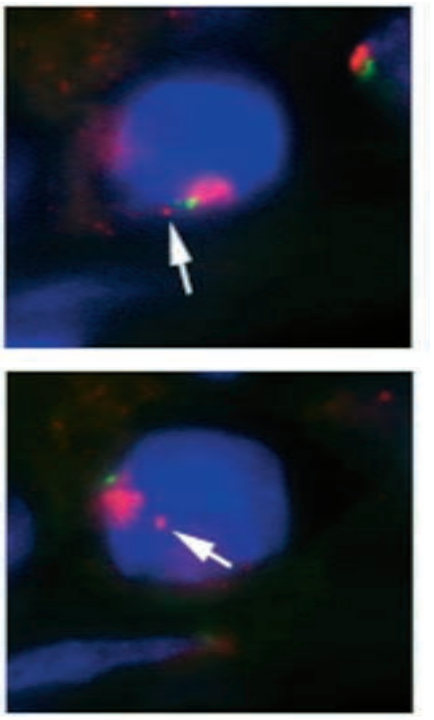

**Fig. 3.** Two representative images of a spermatogonium nucleus at two subsequent light optical sections spaced approx. 4 μm apart. These were obtained by conventional fluorescence microscopy of the same tissue section as shown in Fig. 5. Chromosome 3 q-arm chromatin and p-arm telomeres (arrows) are labeled with (dig/Cy3, red). Peripherally located centromere signals are delineated with FITC (green). Nuclear DNA is counterstained with DAPI (blue) and reveals the nuclear outline and morphology. 3p telomeres are seen as distinct spots separated from the bulk of the q-arm chromatin. 3q-arm chromatin is not revealed because the nuclear counterstain occupies the blue channel. The oblong DAPI-stained structure to the lower left represents the nucleus of a myofibroblast.

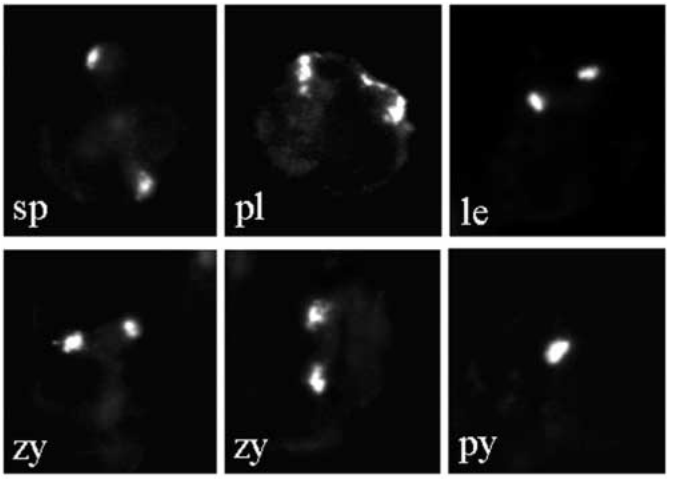


**Fig. 4.** Morphology of FISH signals (FITC, white) of the pericentromeric, chromosome 3-specific, α-satellite DNA probe in nuclei of spermatogonia (sp) and spermatocytes at preleptotene (pl), leptotene (le), zygotene (zy) and pachytene (py). Note that the preleptotene signals line the nuclear periphery. Images were obtained with a standard fluorescence microscope.

least one optical section where the signals of one pair of homologous arms were confluent. To allow for a comparison with values from the unpaired arm signals of the same nucleus, these were summed.

### Chromosome territories in meiotic stem cells

First we wished to examine the morphology and distribution of sub-chromosomal domains in spermatogonia. The latter were identified by their close association with the basal

**Fig. 5.** Representative sequences of confocal light optical sections selected from serial-sectioned nuclei of (a,b) spermatogonia and spermatocytes at various stages of meiotic prophase; (c,d) preleptotene; (e) leptotene; (f,g) zygotene; and (h) pachytene. Labeling and color coding of chromosome 3 subregions is as described in Fig. 1. Sections are generally spaced by 1 μm in the z-direction. (a) Chromosome arm domains appear separated, compact and heavily labeled in spermatogonia. (ai) Top of nucleus with a round centromere (green, arrow) and a 3q-arm domain signal (red). (aii) Two signals each for 3p- (blue) and 3q-arm domains and a second, dumbbell-shaped centromere signal (arrow) are seen. (aiii-v) Sections with a compact 3q-arm domain signal. (b) Spermatogonium at the $G_2$ cell cycle stage. (bi) Upper part of nucleus shows a light optical section through a centromere (arrow) and the 3p- and 3q-arm domains of one homologue. (bii) A signal doublet (arrowhead, enlarged in inset) for the 3q-telomere probe is seen within the corresponding p-arm chromatin and indicates replicated DNA. (biii) p- and q-arm domain signals and aspects of a centromere signal (arrow) of the second homologue are seen. (biv-v) Light optical sections displaying the more flat course of the q-arm domain signal. (c) Preleptotene nucleus, showing an extended q-arm (ci-ii) and its associated peripheral centromeric signal (arrow). Part of the homologous q-arm domain signal is seen below. (ciii) Section showing the large part of the second q-arm domain and the associated centromere signal, which is split up (arrow). (civ,v) Details of p-arm domain signals near bottom of nucleus. (d) Preleptotene nucleus with decondensed centromeric α-satellite DNA signals (arrows in di and iii mark highest signal intensities) and extended, rather dense 3p- and q-arm signals. (e) Leptotene nucleus showing elongated p- and q-arm signal tracks in all details. (ei) A 3p telomere signal (arrowhead) seen at the top of the nucleus marks the end of a 3p-arm domain. (eiv,v) Homologous centromeric signals (arrows) are well separated and compact. (f) Two zygotene nuclei are seen in the selected images of this optical section series. One nucleus is situated at the upper right and signals corresponding to it appear in sections fi-iv. Signals corresponding to a second nucleus extend from the center the lower left in sections fiii-iv. (fi) Telomeres of p-arms are seen at the top of the nucleus (arrowheads). (fii) Separate, dumbbell shaped centromere signals (short arrows) are seen with their corresponding p-arms. Note the distinguishable sister chromatids. (fiii) Details of pairing forks for q-arms of both nuclei. A telomeric signal (blue, arrowhead) locates at the end of the signal track of the lower q-arms. (fiv) Separate centromeres of the lower nucleus (long arrows), while two 3p telomere signals are seen to the left (arrowhead). (fv) A single, prominent telomere signal (arrowhead) is seen at the termini of signal tracts for the homologous p-arm domains, which appear aligned. (g) Light optical sections of a zygotene spermatocyte. One signal for 3p-telomere (gi, arrowhead; top of nucleus) and 3p-arms (gi-v) is seen and indicates pairing. (giii-v) 3q-arms are bent but distant. 3q telomeres are situated at the nuclear periphery (giv,v, arrowheads). Note: this nucleus was taken from a different set of experiments where centromere probes were not present. (h) Optical sections of a pachytene spermatocyte. The bivalent exhibits a hook shape, with the telomeres located close to each other at the lower left (hiii,iv, arrowheads). (hii,iv) Details of the course of signal tracks of individual homologues can be discriminated.

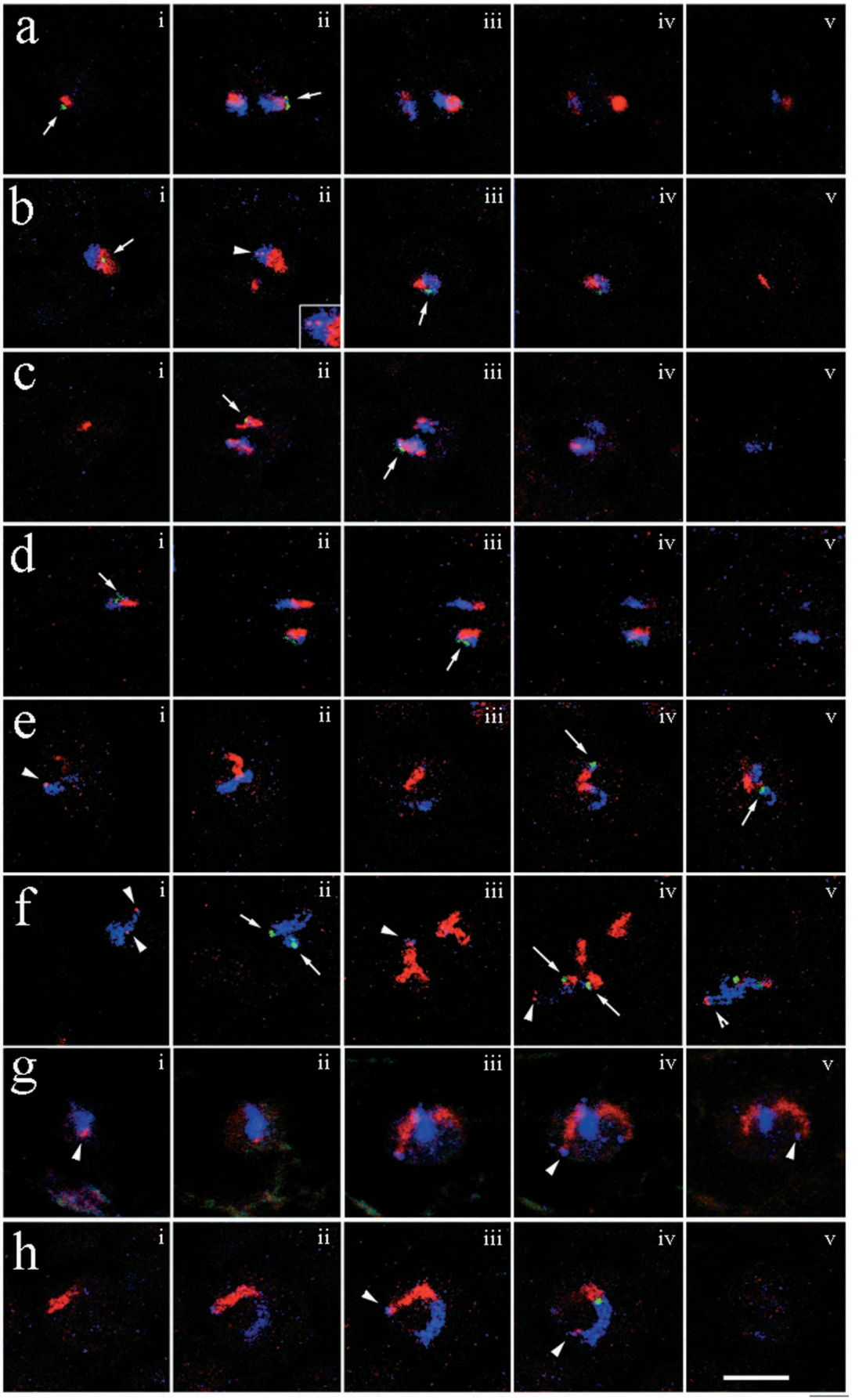
a
b
c
d
e
f
g
h
i
ii
iii
iv
v

**Table 1. Mean values of volumes, surface area and roundness factor obtained for chromosome 3p- and 3q-arm territories**

| Parameter | Stage | Chromosome territory 3p* | 3q* | 3p+3q† |
|---|---|---|---|---|
| Volume ($\mu m^3$) | Spermatogonia (*n*=20) | 13.5 (±5.8) | 14.4 (±4.7) | 27.81 (±10.2) |
| | Preleptotene (*n*=22) | 15.6 (±3,9) | 18.6 (±4.9) | 34.21 (±6.4) |
| | Leptotene (*n*=16) | 15 (±4.8) | 16.6 (±5.6) | 31.54 (±8.3) |
| | Zygotene (*n*=11) | 16.3 (±7.9) | 20 (±10.4) | 36.27 (±15.7) |
| | Pachytene (*n*=9) | 12.2 (±4.4) | 16.4 (±6.1) | 28.62 (±6.4) |
| Surface area ($\mu m^2$) | Spermatogonia | 76.6 (±21.8) | 68.62 (±14.7) | 145.2 (±35.3) |
| | Preleptotene | 88.6 (±18.8) | 94.0 (±17.1) | 182.6 (±38.2) |
| | Leptotene | 96 (±20) | 91.1 (±17.9) | 188 (±22.1) |
| | Zygotene | 91.5 (±26.7) | 98.5 (±41.2) | 190 (±61.4) |
| | Pachytene | 72.6 (±17.4) | 71.4 (±16.4) | 144 (±16.8) |
| Roundness factor | Spermatogonia | 0.078 (±0.028) | 0.140 (±0.032) | |
| | Preleptotene | 0.085 (±0.033) | 0.099 (±0.037) | |
| | Leptotene | 0.062 (±0.027) | 0.080 (±0.026) | |
| | Zygotene | 0.039 (±0.014) | 0.052 (±0.025) | |
| | Pachytene | 0.044 (±0.012) | 0.083 (±0.024) | |

*p and q values are the sum of both arm-domain signals of a nucleus (Spermatogonia - zygotene).
†3p+q denotes the summed chromosome 3p,q values/nucleus.
*n*, number of signals of the respective arm domain.
Standard deviation is given in parentheses.

membrane of the testis tubule (Fig. 2). Inspection of hybridization signals in images obtained by conventional fluorescence microscopy revealed that this cell type predominantly displays compacted and separate domains of p- and q-arms of chromosomes 3 (Fig. 3). Since conventional fluorescence images usually represent two-dimensional projections of FISH signals, several spermatogonia were subjected to light optical serial sectioning. In 11 serially sectioned spermatogonia (*n*=13), homologous chromosome territories were of variable shape and spatially separate (Figs 5a,b, 6a,b). Chromosome arm domains were detected as compact, intensely labeled individual subchromosomal compartments (Figs 4, 5a,b, 6a,b). In one nucleus the chromatin of p-arms was associated, while in a second spermatogonium the q-arm chromatin signals were associated; i.e. there were at least one or two light optical sections with a continuous signal area. Hence, homologues and their arm domains were separated from each other in 85% of cells, an observation which is in accordance with the spatial arrangement of chromosome 1 territories in human, and chromosome 8 and 12 subsatellite domains in mouse spermatogonia (Scherthan et al., 1996). Spatially separated and compacted homologous arm domains were detected in spermatogonia nuclei, which displayed a $G_1$ signal pattern (i.e. a single signal/centromere, Figs 3, 4) as well as in nuclei with a $G_2$ signal pattern for the pericentromeric/telomeric DNA probes (Fig. 5bii), i.e. a signal doublet/target region (see Selig et al., 1992).

Three-dimensional reconstruction (Fig. 6) and quantitative image analysis of 3p- and q-arm domain signals revealed a considerable intra- and internuclear variation of volume, surface area and roundness factor estimates (Table 1). The roundness factor is indicative of the shape of a territory. A larger roundness factor corresponds to a smoother surface and/or rounder territory. Volumes and surface areas of arm domains could differ between homologous arms in a particular nucleus (not shown), and between the large and short arm of the same chromosome (Table 2). In summary, one can conclude that premeiotic chromosome-arm chromatin occupies distinct domains within variably shaped interphase chromosome territories. These observations are consistent with the variable arrangement of human chromosome 3 arm domains in human amniotic fluid cells (Dietzel et al., 1998).

Chromosome 3 pericentromeric signals obtained with the α-satellite DNA probe were also of variable morphology (Figs 4, 5a,b) and formed a distinct domain within a chromosome territory, with a fraction of the α-satellite domain always constituting a part of the territory surface (Fig. 6a,b). Pericentromeric signals were generally oriented towards the nuclear periphery (Figs 3, 4), away from the nuclear center (compare Figs 5a,b and 6a,b). Mathematical analysis of pericentromeric signals revealed a considerable intra- and internuclear variation of centromere domain volumes (Table 3).

**Table 2. Mean values of 3p/3q ratios of volumes and surface area at a given stage**

| Ratios 3p/3q | Volume | Surface area |
|---|---|---|
| Spermatogonia | 0.96 (±0.30) | 1.13 (±0.26) |
| Preleptotene | 0.89 (±0.45) | 0.97 (±0.37) |
| Leptotene | 1.06 (±0.52) | 1.16 (±0.53) |
| Zygotene | 0.94 (±0.47) | 0.99 (±0.33) |
| Pachytene | 0.90 (±0.41) | 1.12 (±0.36) |

The values are based on those of Table 1.
Standard deviation is given in parentheses.

**Table 3. Mean volumes of α-satellite signals at chromosome 3 pericentromeres at a given stage**

| Stage (no. of signals) | Volume ($\mu m^3\ 10^{-2}$) |
|---|---|
| Spermatogonia (22) | 64.7 (±40.6) |
| Preleptotene (18) | 53.1 (±20.1) |
| Leptotene (16) | 57.1 (±9.9) |
| Zygotene (20) | 81.2 (±32.6) |
| Pachytene (10) | 175.8 (±77.1) |

Standard deviation is given in parentheses.

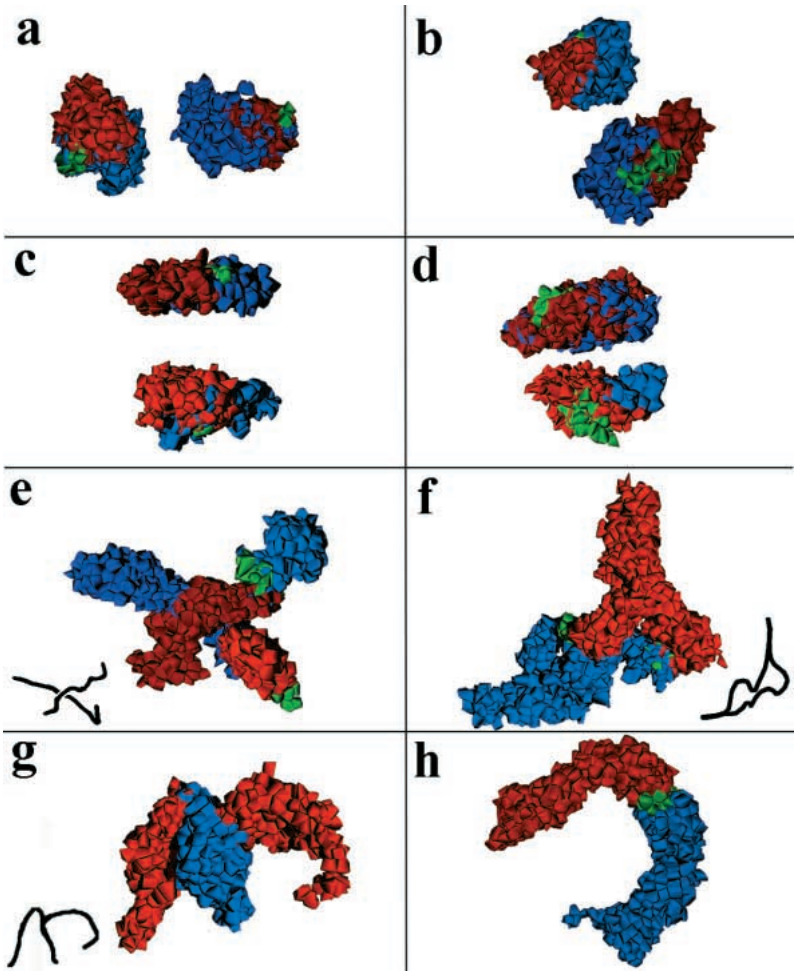


**Fig. 6.** Three-dimensional reconstruction of p-arm, q-arm and centromeric domains derived from the complete confocal image stacks of the nuclei shown in Fig. 4 by the Voronoi tessellation procedure. Short arm domains are shown in blue, long arms in red and centromeres in green. Since telomere signals are not seen at the surface of reconstructed spermatogonia, so for the sake of a clear display these are not shown. (a,b) Spermatogonia exhibit a compacted shape, with part of the centromeric α-satellite DNA signal comprising a segment of the domain surface. The dumbbell shape of the centromeric domain of the lower territory in b indicates replicated DNA, which is consistent with the corresponding telomere signal pattern seen Fig. 4b. (c,d) Preleptotene nuclei with separate chromosome 3 territories. The elongated nature of the chromosome arms is not clearly evident because these are folded back onto each other. Note the large centromeric domains in d, indicating preleptotene (see text). (e) Leptotene nucleus. Chromosomes display an outstretched shape. The two chromosomes are arranged such that they lie perpendicular to each other and that non-homologous arm chromatin is traversed. Line drawing at the lower left indicates the course of homologues. (f) Zygotene nucleus; chromosomes corresponding to lower left nucleus in Fig. 4f are shown. Homologous arm domains are in contact at the terminal parts, while centromeric regions are still separate. See line drawing for the course of homologues. (g) Zygotene chromosomes corresponding to Fig. 4g. Pairing has initiated at short arm telomeric regions, while long arms are bent and still widely separate. Note: this nucleus was taken from a different set of experiments without centromere probes, therefore these are not shown. (h) U-shaped pachytene bivalent showing complete pairing of homologous chromosome domains.

### Distribution of 3p,q telomeric regions in spermatogonia

The labeling scheme for chromosomes 3 also included specific YAC probes for p- and q-arm telomeric regions (Fig. 1). Inspection of the optical sections of each nucleus allowed the interactive identification of telomeric signals, provided that such a signal was distant from the similarly labeled chromatin of the opposite chromosome arm (Figs 3, 5bii). Probably for this reason (see Discussion), 3p,q telomeric regions were detected in similar frequencies but only in about 40% of the chromosome arm domains investigated ($n$=40).

Image analysis was applied to compute the gravity centers of the identified telomere signals and the distance to the nearest domain surface. It was found that the telomere signal gravity centers were predominantly below the surface of the chromatin cloud marking the 3-D extension of the particular arm domain (Fig. 7). In spermatogonia, diameters of a few signals measured up to 0.8 μm. Therefore, in most cases the chromatin stained by the telomeric YAC probes was embedded in arm-domain chromatin.

### Chromosome territories are restructured during preleptotene

Post-replicative human preleptotene nuclei display a unique α-satellite DNA distribution, such that the centromeric α-satellite DNA appears to line the nuclear envelope (Scherthan et al., 1996). In the present study, nuclei were scored as preleptotene when both chromosome 3 pericentromeric α-satellite signals were decondensed and located at the nuclear periphery (Figs 4, 5c,d).

In the preleptotene nuclei investigated by confocal laser scanning microscopy (CLSM) ($n$=11), homologous chromosome arm domains were remote from each other and not aligned (Figs 5c,d, 6c,d). Generally, two of the four chromosome 3-arm domains within a nucleus showed an elongated morphology (Fig. 5c,d). Statistical analysis of the data derived from the confocal image stacks using the Kolmogorov-Smirnov two sample test (Young, 1977) revealed that arm-domain volumes from spermatogonia and preleptotene spermatocytes did not differ significantly (Table 4). Variation between individual nuclei was considerable and made up to some 30-40% of volumes. A highly significant increase in surface area estimates of preleptotene arm domains as compared to those of spermatogonia (Table 4) indicated a change towards an elongated shape and/or a more complex surface structure. While preleptotene roundness factor values did not significantly differ from that of spermatogonia, cumulative frequency curves, however, revealed an intermediate distribution between spermatogonia and leptotene values (Fig. 8c). Furthermore, a considerable difference of

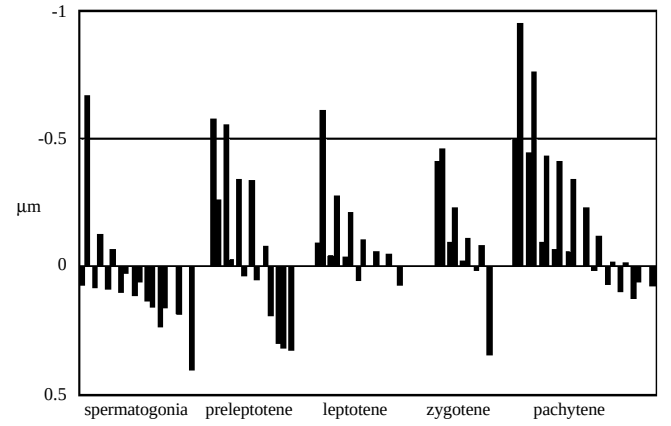


**Fig. 7.** Distances (in µm) of gravity centers of telomeric signals with respect to the nearest arm-domain surface, indicated according to the extension of bars above or below '0', which denotes the surface of the arm-domain chromatin. Bars below this line indicate that signal centers locate either inside (positive values) or outside (negative values) of the arm domain surface. It should be noted that signal gravity center distribution does not indicate whether signals were in contact with the domain surface. In spermatogonia the diameter of a few signals measured ≤ 0.8 µm. The large bar at the second position from the left was created by a telomere signal which was surrounded by a small rim of 3p-arm chromatin that was external to the bulk of the arm-domain chromatin. Pachytene telomere signals were generally larger in diameter (>1 µm), which results in larger distances between signal centers and corresponding arm-domain surfaces. Stages of nuclei are indicated below the respective group of values.

roundness factor estimates was noted between homologous arm domains in individual nuclei (Table 1). This suggests that the elongation of homologous chromosomes initiates during preleptotene and is not tightly synchronized. In contrast, differences between roundness factor values of homologous arm domains in individual spermatogonia or leptotene nuclei were less pronounced (Table 1).

## Preleptotene nuclei display an altered telomere distribution

At preleptotene, 54% of gravity centers of 3p and 3q telomeric signals (*n*=13) located above the signal boundary of the respective chromosome arm-domain chromatin (Fig. 7). This contrasts with 3p,q telomere distribution in spermatogonia, where 81% of signal centers of telomeric probes were detected within the signal cloud of the respective chromosome arm domain chromatin. The difference in telomere distribution between stem cells and preleptotene spermatocytes is most likely associated with a general reorganization of chromosome and nuclear architecture during this stage (see Discussion).

**Table 4. Significance levels for differences between values diagnostic of 3p- and 3q-arm domain morphology as computed by the two-sided Kolmogorov-Smirnov test (Young, 1977)**

| | Meiotic stage | | |
|---|---|---|---|
| Parameter | Spgon-Prelep | Spgon-Lepto | Prelep-Lepto |
| Volume | 0.05 | >0.1 | >0.1 |
| Surface | **0.001** | **0.001** | >0.1 |
| Roundness factor | >0.1 | **0.005** | 0.05 |

Spgon, spermatogonia; Prelep, preleptotene; Lepto, leptotene.

Significance levels for zygotene and pachytene could not be computed, since the number of data points (arm domains) after initiation of pairing was too small.

Bold figures denote highly significant differences.

## Leptotene chromosome organization

The analysis of the spatial arrangement of leptotene chromosomes seemed particularly important to us, since serial section electron microscopy (EM) failed to trace the axial cores of human leptotene chromosomes near the centromeric regions (Rasmussen and Holm, 1978; Boiko, 1983). Moreover, knowledge of the spatial distribution of the chromatin of homologues is crucial for an understanding of the homology search and alignment process. Leptotene cells, which are in the adluminal compartment of the tubule membrane, were identified by the threadlike appearance of differentially colored and misaligned chromosome territories (Figs 5e, 9) and thread-like appearance of their DAPI-stained chromatin (not shown).

The differentially colored FISH signals along chromosomes 3 allowed us to deduce the orientation of the two homologues with respect to each other. It was found that leptotene chromosomes were frequently misaligned (Fig. 9a,b). In 15 serially sectioned nuclei the two homologues spanned the nuclear lumen in various aspects of bent conformations, typically without touching each other or touching at nonhomologous regions (Figs 6e, 9, 10). Distance alignment, i.e. an obvious spatial coorientation of unpaired homologues was only seen in one nucleus (Fig. 9c). Similar observations were made by conventional fluorescence microscopy in testis tissue sections as well as in formaldehyde-fixed cells from testicular suspensions (H. S., unpublished data). The significance of the detection of spatially separated leptotene chromosome territories is underlined by the fact that, according to signal distribution, the partial or overall premeiotic association of homologues should have led to the confluence of arm signals and consequently to classification as zygotene or pachytene.

In leptotene nuclei, homologous chromosome ends were far apart (Figs 6e, 9) and were seen at the nuclear periphery of confocal raw images (see Fig. 5g) and images obtained by conventional fluorescence microscopy (not shown). Peripheral and distant location of homologous leptotene telomeres is consistent with the serial section EM analysis (Rasmussen and Holm, 1978; Boiko, 1983). Telomere signal gravity centers were situated adjacent to or at the terminal surface of the outstretched leptotene arm domains (Figs 7, 9).

Pericentromeres were consistently of compacted, more or less ovoid shape (Figs 4, 5eiv,v). Signal volumes were of considerable homogeneity, as shown by quantitative image analysis (Table 3). These observations contrast with preleptotene pericentromere signal morphology (Fig. 4) and the more variable signal volumes observed at other stages.

Mathematical analysis of 3p- and 3q-arm domains revealed similar volumes in spermatogonia, preleptotene and leptotene nuclei (Tables 1, 4). However, as compared to spermatogonia, estimates of surface area showed a highly significant increase at leptotene, while roundness factors showed a highly significant drop (Table 4, Fig. 8). This drop indicates the restructuring of chromosome 3 territories and their arm domains towards a more elongated shape with a more complex surface structure.

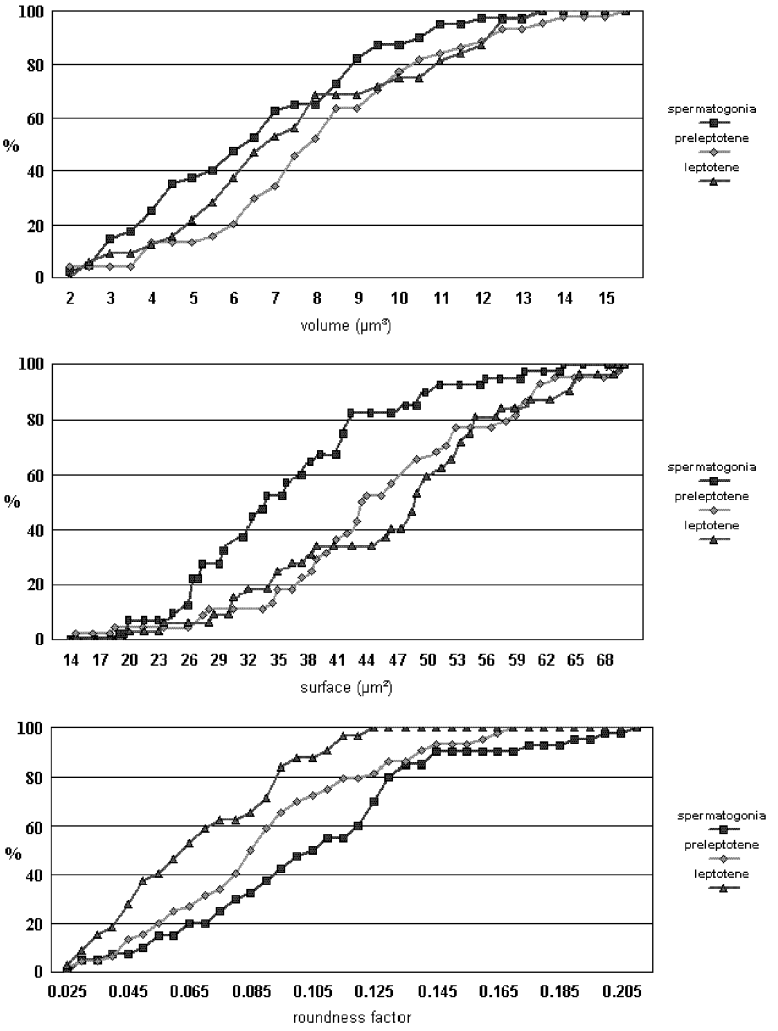


**Fig. 8.** Cumulative graphs of absolute values computed for the morphological parameters of the chromosome 3 territories of spermatogonia, preleptotene and leptotene phases derived from the summed 3p- and 3q-arm domain data given in Table 1. The estimates are assorted according to their increasing magnitude along the x-axis. The maximum data number equals 100%. The surface area of preleptotene and leptotene chromosomes is significantly shifted towards higher values as compared to spermatogonia. Consistent with more compact chromosome territories in spermatogonia, their RF estimates are larger than those in preleptotene and leptotene. The intermediate position of preleptotene RF values indicates that elongation of chromosome territories commences during this stage.

An overall chromosome condensation with decreased volumes and surface areas was not apparent for the premeiotic interphase/leptotene transition.

### Leptotene chromosomes show intimate chromatin contacts

The triple-color labeling of chromosome 3 homologues also provided a unique opportunity to scrutinize the interaction of the chromatin of leptotene chromosomes. This was possible in cells where the differentially labeled non-homologous chromatin of the p- and q-arms touched each other. Signal areas that contain chromatin from heterologous arm domains can be identified by a mixed color. In at least two such cases color overlap was seen in four consecutive raw sections (covering 1 µm in the z-direction) of the nucleus (Fig. 10), which indicates significant intermingling of non-homologous chromatin and suggests that contacts between leptotene chromosomes are not restricted to the territory surface. Moreover, close to the compacted leptotene centromeres sister chromatids could be discerned as juxtaposed signal tracts (Fig. 10).

### Zygotene chromosomes display a unique chromosome morphology

Zygotene nuclei were identified by their fiber-like chromatin upon DAPI staining (not shown) and the partial pairing of hook-shaped chromosome 3 signals (Fig. 6f,g). Out of 15 optically serial sectioned nuclei, 3 showed intimate chromatin pairing initiating at the ends of the short arms, 6 at the ends of long arms and in another 6 nuclei pairing had initiated at the telomeres of both arms (Figs 5f,g, 6f,g). In nuclei where pairing initiated from one end, the unpaired arm domains were still far apart (Fig. 6g). Terminal pairing initiation is in agreement with earlier studies (Rasmussen and Holm, 1978; Barlow and Hultén, 1997). Three-dimensional reconstruction showed a reduced diameter of chromosome signal tracts at the telomeric regions (Fig. 6f,g), which may relate to shorter DNA loops at the termini of mammalian pachytene chromosomes (Heng et al., 1996).

Telomeric YAC signals were usually found at the end of the arm domains from leptotene to pachytene (Fig. 5e-h), and gravity centers of telomeric signals located predominantly adjacent to the nearest domain surface (Fig. 7). Zygotene pericentromeric signals were often dumbbell-shaped and more irregular as compared to leptotene signals (Figs 4, 11c). A considerable variation of volume values between intra- and internuclear pericentromeres was apparent and volumes estimates had significantly increased over leptotene values (Table 3).

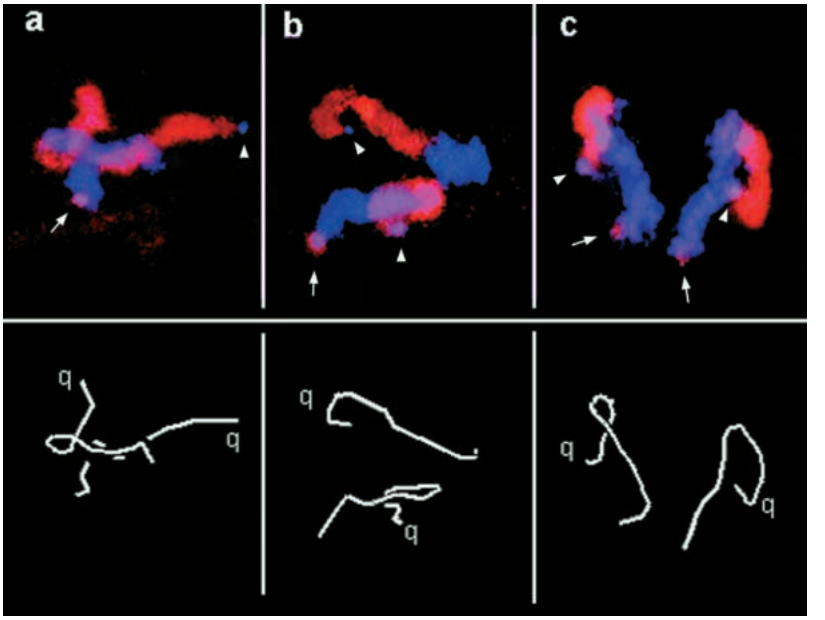


**Fig. 9.** Spatial arrangement of differentially labeled chromosomes 3 in three leptotene nuclei. The images are projections of confocal serial sections. q-arms are labeled in red (rhodamine), p-arms in blue, while the telomeres of the same arm are inversely labeled (arrows); telomeres of the long arm are denoted by arrowheads. The line drawings below the confocal image indicate the course of signal tracks. The relative position of the respective q-arms is indicated as '*q*'. (a) Homologous arms are far apart, with the blue signal of the p-arm of one homologue projected over the red (pink color) of the q-arms of both homologues. Chromosomes are misaligned. The pink point to the left (arrow) represents a 3p telomere signal, while the small blue dot to the right marks the 3q telomere of the same chromosome (arrowhead). (b) Leptotene chromosomes in anti-parallel arrangement, with non-homologous chromatin in contact. The telomeres of the lower chromosome are heavily labeled, while the 3q telomere signal of the homologue is small (arrowhead). (c) Distance alignment of U-shaped chromosomes. Stretched p-arms and their telomeres (arrows) are seen in parallel in the foreground, while 3q-arms are profoundly bent and telomeres (pink, arrowheads) locate to the side of the nucleus. It should be noted that the telomeres of all nuclei shown were positioned at the nuclear periphery (not shown).

The well-preserved nuclear structure obtained in the current FISH experiments allowed us to analyze the chromatin conformation associated with the onset of synaptic pairing. Inspection of the optical sections revealed that human zygotene chromosomes display an irregular surface structure with discernible sister chromatids along unpaired chromosome regions (Fig. 11). This increase in surface complexity is mirrored by a considerable drop of roundness factor estimates of arm domains (Table 1). While mean surface area estimates were in the range of leptotene values, volume estimates were at their maximum at zygotene, with the difference from previous stages being modest (Table 1). To determine any statistical relevance of volume differences in chromosome 3-arm domains between leptotene and zygotene, volume estimates of zygotene were bisected. These values were regarded as individual arm domains. It was found that the difference between the volume estimates of leptotene and zygotene arm domains was not statistically significant ($P$>0.1).

## Chromosomes condense at pachytene

A single, differentially colored and generally U-shaped signal tract meandering through the nuclei of pachytene spermatocytes demonstrated complete pairing of homologues (Figs 4h, 5h). Chromosome arm-domain volume and surface area estimates were reduced as compared to zygotene and were again in the range of that of spermatogonia, while roundness factor estimates had considerably increased (Table 1). Pachytene telomere signals were of dumbbell shape and always

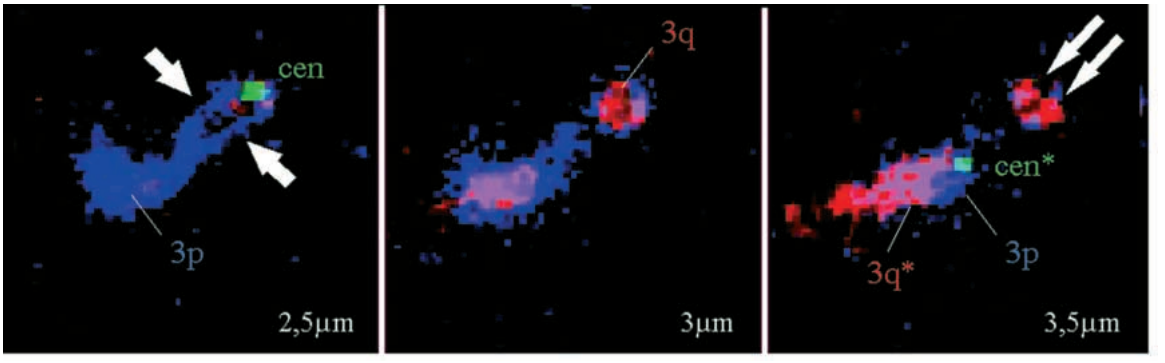


**Fig. 10.** Aspects of chromatin interactions of leptotene chromosomes. Three selected confocal light optical sections are shown at high magnification. Contrast and brightness were enhanced to facilitate display. Positions of sections in the z-direction are indicated to the lower right and probes are identified in the image by the respective color. Chromosome 3 domains are designated by the corresponding abbreviations. The domains of the second chromosome are marked with an asterisk. In the optical sections at 2.5 and 3.5 µm sister chromatids of a p- and q-arm can be observed as separate signal tracks (arrows) near the centromere regions (cen, green) of the homologues. In the 3 and 3.5 µm section a pink color patch indicates that this area contains chromatin of non-homologous chromosome arms from different chromosomes. Centromeric signals (green) appear as small, compacted areas.

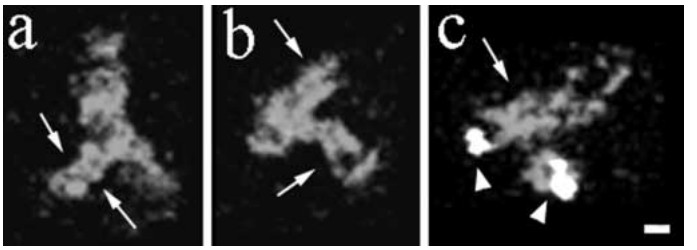


**Fig. 11.** Details of confocal images of zygotene chromosomes shown in Fig. 4 at high magnification. (a-c) Unpaired regions of homologous chromosome arms display a jagged, twin-stranded morphology. Arrows are drawn perpendicular to regions where sister chromatids can be discerned. (a,c) The chromatin of the homologous arms appears in a chromomeric pattern with thinner and more compacted regions alternating. (c) Separate centromeric signals are dumbbell shaped (white; arrowheads). Bar, 1 μm.

found at the ends of signal tracks (Fig. 5hiii,iv). Pericentromeric signals were large and variably shaped. Volume estimates were the highest of all stages investigated: due to homologue paring volumes had doubled as compared to zygotene (Table 3) but a threefold increase over leptotene values was still up.

## DISCUSSION

We have analyzed the three-dimensional arrangement and organization of the chromatin of homologous chromosomes 3 prior to and during the onset of male meiotic prophase. The experiments were facilitated by the extended leptotene stage in the human (Adler, 1996) and the excellent performance of human subregional chromosome paint probes (Guan et al., 1996) in tissue section FISH. The results obtained provide the first quantitative and structural description of the three-dimensional remodeling and reorientation of homologous chromosome territories and their sub-domains during the course of earliest meiotic prophase.

### Chromosome architecture and distribution in spermatogonia

The analysis of chromosome distribution and morphology in spermatogonia showed that the homologous chromosomes 3 are sectored in separate arm domains of variable shape. Besides a flexible folding of the chromatin fiber within chromosome territories and arm domains (Yokota et al., 1995; Dietzel et al., 1998; Zink et al., 1998), the variations in shape could to some extent reflect distinct transcriptional activities at particular cell cycle and/or differentiation stages (for a review see Jackson and Cook, 1995). Chromosome 3 territories were predominantly spatially separated in meiotic stem cells as well as in preleptotene nuclei, which suggests that they maintain their preferential spatial arrangement beyond premeiotic S-phase. Individual chromosome territories were also observed in human and mouse spermatogonia (Scherthan et al., 1996), human amniotic fluid cells (Dietzel et al., 1998), in myofibroblasts and Leydig cells (H. S. and S. D., unpublished data). In a stable disomic maize-chromosome-addition line of oat 3D-GISH revealed that at premeiotic interphase the territories of the pair of maize homologues were of more or less compact shape, with seemingly random positions within the nucleus (H. W. Bass, personal communication). Premeiotic association of homologues has been detected in cereals (Aragón-Alcaide et al., 1997; Schwarzacher, 1997) and yeasts (Loidl et al., 1994; Scherthan et al., 1994; Weiner and Kleckner, 1994) and seems to profit from centromere clustering, i.e. a Rabl organization of premeiotic chromosomes (Funabiki et al., 1993; Aragón-Alcaide et al., 1997; Schwarzacher, 1997; Jin et al., 1998). In human fibroblasts and HeLa cells, the spatial distribution of homologues seems to be regulated in some way, since these appear to be organized in antiparallel haploid sets at mitotic prophase (Nagele et al., 1995). It will be interesting to determine whether such an arrangement is present in meiotic prophase, because the ordered distribution of parental complements would facilitate homologue alignment at leptotene.

Signals of pericentromeric domains of chromosomes 3 were also of variable shape and volume in spermatogonia. A fraction of the α-satellite DNA signal consistently formed a part of the chromosome 3 territory surface, with the signals in all nuclei analyzed being oriented towards the nuclear periphery, away from the nuclear center. This signal arrangement may relate to the preferential association of pericentromeric, late-replicating heterochromatin with the nuclear periphery (see e.g. Comings, 1980; Ferguson and Ward, 1992; Ferreira et al., 1997).

In spermatogonia, 3p and 3q telomeric signal centers located predominantly in the nuclear interior and were embedded in arm-domain chromatin. The intra-nuclear distribution is in agreement with the scattered three-dimensional distribution of telomeres in mouse and human spermatogonia (Scherthan et al., 1996; Zalensky et al., 1997) as well as somatic mouse cells (Vourc'h et al., 1993). The histological staging applied in this study did not distinguish resting from more differentiated spermatogonia. Thus, our category of spermatogonia will include stem cells at various developmental stages and thus cannot indicate more than a general trend for the distribution of chromosome 3 telomeric regions in this cell type.

The theoretical number (4) of chromosome 3 telomeres present in a nucleus was rarely observed. We ascribe this effect to the accidental location of telomere YAC signals near the similarly colored chromatin of the opposite chromosome arm of the same homologue, which agrees with the highly variable arrangement of chromosome 3 telomeric regions with respect to each other in somatic nuclei (Dietzel et al., 1998). Since the available CLSM allowed only the excitation of up to three different fluorochromes, telomere probes could not be marked in further colors for their unequivocal detection. It can, after all, not be excluded that due to a small signal size some telomere signals went unnoticed. Future developments of multi-color FISH schemes for three-dimensional chromosome analysis should allow for the unequivocal delineation of more than three target regions of a chromosome (or several chromosomes) within a nucleus and thereby further expand our knowledge of chromosome organization in somatic and meiotic cells.

### Chromosome territories are reorganized during preleptotene

Prepleptotene chromosome 3 territories displayed volumes

similar to spermatogonia. Surface area estimates, however, showed a highly significant increase as compared to spermatogonia values, while roundness factor estimates, as displayed by cumulative frequency curves, adopted an intermediate position between spermatogonia and leptotene values (Fig. 8). The observed changes towards larger surface area and reduced roundness factor estimates suggest that elongation of chromosome territories and their subdomains initiates during preleptotene. Pronounced variations of roundness factor estimates between homologous arm domains of individual nuclei indicate that the elongation of chromosomes commences asynchronously during preleptotene. Since chromosome territories were still separate from each other during this stage, chromosome remodeling seems not to be linked to homology search, but rather may relate to their reorganization from a flexibly folded interphase chromosome within somatic chromosome territories (Sachs et al., 1995; Dietzel et al., 1998) into the stretched out leptotene territories, which have their DNA loops attached to a more rigid axial core (see Moens and Pearlman, 1988). It can also be envisaged that the observed changes are associated with an increased transcriptional activity (Cook, 1997).

Three-dimensional analysis revealed, furthermore, that more than half of the chromosome 3 telomeric signal centers were seen adjacent to the surface of the respective arm domains, which suggests that telomere distribution is also modified during preleptotene. In spermatogonia telomeric regions seem to be embedded in chromosome-arm domain chromatin, while these obtain a more exterior location at preleptotene. This switch in distribution could be the consequence of an increased chance of a signal center lying near to the surface of an elongated domain (due to a reduced diameter of the latter), and furthermore, relates to the general telomere redistribution towards the nuclear envelope occurring during the onset of meiotic prophase in mouse and man (Scherthan et al., 1996) fission yeast (Chikashige et al., 1994, 1997) and maize (Bass et al., 1997).

### Leptotene chromosome organization

The differential coloring of chromosome 3 territories revealed that leptotene chromosomes were spatially separated and variably oriented with respect to each other. This indicates that proper prealignment of homologues requires large-scale chromosome movements during leptotene, which are probably different from the restricted Brownian chromosome motions that were recently observed in live somatic cells (e.g. Marshall et al., 1997; Zink et al., 1998). Saltatory rotations and other nuclear movements have been noticed during early stages of meiotic prophase of the rat (Parvinnen and Söderström, 1976; Salonen et al., 1982) and fission yeast (Chikashige et al., 1994; Svoboda et al., 1995). Several studies suggest that chromosome pairing at meiosis involves a tubulin-dependent mechanism acting at meiotic telomeres (see Loidl, 1990; Dernburg et al., 1995, for reviews). In support of this assumption it has been shown that in fission yeast, microtubules drive spindle-pole-attached telomeres and by this the nuclear motions during karyogamy and meiotic prophase (Ding et al., 1998). Furthermore, mutation of the microtubule-dependent motor protein *KAR3* impairs synapsis and recombination in budding yeast (Bascom-Slack and Dawson, 1996).

Misaligned leptotene chromosome showed considerable intermingling of non-homologous arm-domain chromatin, which is generally not observed for somatic chromosome territories (see Cremer et al., 1993; Kurz et al., 1996). Such extensive chromatin interactions during leptotene may contribute to genome-wide homology testing and represent the physical basis of efficient ectopic recombination (e.g. Jinks-Robertson and Petes, 1985; Haber et al., 1991; Murti et al., 1994; Goldman and Lichten, 1996). The elongation of chromosome territories and assembly of axial cores prior to homologue search may be required to confer sufficient rigidity to meiotic chromosomes to withstand the shearing forces imposed when chromosome ends are gathering at a limited sector of the nuclear envelope to form a chromosomal bouquet in the leptotene/zygotene nucleus. The observation in mammals that elongation of chromosome territories occurs prior to alignment and synapsis is consistent with the view that bouquet formation could be the underlying mechanism for a recombination-independent alignment process (for recent reviews see Kohli, 1994; Cook, 1997; Roeder, 1997; Scherthan, 1997).

Homology testing may occur at multiple sites and may involve contacts between intact double helices (Kleckner and Weiner, 1993; Kleckner, 1996) or DNA/DNA interactions mediated by single-stranded feelers (Smithies and Powers, 1986; Carpenter, 1987), possibly at DNase I hypersensitive sites (Wu and Lichten, 1994) that are heavily engaged in transcription (Cook, 1997). Homology testing at the DNA level may involve RecA homologues and mismatch repair proteins (Bishop, 1994; Ashley et al., 1995; Baker et al., 1995; Rockmill et al., 1995; Terasawsa et al., 1995; Baumann et al., 1996), which are probably components of early meiotic nodules (Anderson et al., 1997; Barlow et al., 1997; Plug et al., 1998). The high density of coding sequences encountered at human telomeres (Craig and Bickmore, 1994) could facilitate homology recognition (Radman and Wagner, 1993) and initiation of synaptic pairing at these regions (Rasmussen and Holm, 1978; Barlow and Hultén, 1996; this investigation).

### Pericentromeric satellite DNA compaction during homologue search

Compacted morphology and rather uniform volumes of the pericentromeric α-satellite signals at leptotene contrasted with a considerable variability at other meiotic prophase stages. While leptotene pericentromeres generally showed a single-spot signal morphology suggestive of tight sister chromatid cohesion, the adjacent sister chromatid regions were sometimes seen as discrete FISH signal tracks. A reduced sister chromatid cohesion due to the absence of axial cores around pericentromeric regions of human leptotene chromosomes (Rasmussen and Holm, 1978) could be the reason for this effect. The uniform compaction of the pericentromeric heterochromatin at leptotene, on the other hand, could be mediated by a temporary association of pericentromeric α-satellite DNA with heterochromatin-specific meiotic proteins (see Smith and Benavente, 1995) and the general compaction of heterochromatic segments into leptotene chromomeres (e.g. John, 1990). Chromomeres of human pachytene chromosomes are AT-rich and correspond to the G-bands of metaphase chromosomes (Ambros and Sumner, 1987; Luciani et al., 1988). The tight compaction of chromosomal domains enriched in repetitive DNAs may thus relate to mechanisms that prevent the participation of ubiquitously distributed

repetitive sequences from homology search. This agrees with the view that heterochromatin initially may not be involved in homologue alignment and pairing initiation (see Maguire, 1972). However, the association of heterochromatin later at meiotic prophase appears to be crucial for the segregation of achiasmate bivalents (see Dernburg et al., 1996; Karpen et al., 1996).

### Zygotene chromosomes display a unique chromatin morphology

We have observed that the reorganization of chromosome territories, which commences during preleptotene, leads to a highly significant increase in surface area estimates between spermatogonia and preleptotene, and between spermatogonia and leptotene, as well as a highly significant drop of roundness factor estimates between spermatogonia and leptotene arm domains. A significant difference between leptotene and zygotene values was not observed. Hence, a chromosome 'condensation' from leptotene into zygotene, i.e. a reduction in chromatin volume (see Cook, 1997), was not apparent.

A transition from a more rod-shaped leptotene morphology towards a twin-stranded chromomeric morphology, which was noted for painted zygotene chromosomes engaged in synaptic pairing, was mirrored by a considerable drop of roundness factor between leptotene and zygotene. Such a morphology change is associated with synaptic pairing in a variety of organisms (for references see Rhoades, 1961; Dawe et al., 1994). The discernible sister chromatids at this stage seem to be the consequence of the relocation of the axial core lateral to the chromatin of the chromosomes, which is required for assembly of the tripartite SC structure between homologues (von Wettstein et al., 1984). If one assumes that synapsis in the human male initiates predominantly at chromosome ends and spreads in a zipper-like fashion from these sites, it is unlikely that the observed change in chromatin morphology is associated with homology search, but rather that it reflects the physical requirements of tripartite SC assembly. It will, however, be necessary to determine the chromatin conformation of a non-aligned chromosome pair within a human zygotene nucleus and to study chromosome territory structure in other species to clarify this issue.

The shift from a single- to a twin-fiber chromosome morphology during maize pre-zygotene just before intimate (synaptic) homologue pairing was associated with a drastic increase in chromosomal volume (Dawe et al., 1994), while during zygotene chromosome and nuclear volumes reduced again. In the present study we observed similar chromosome volumes between preleptotene and zygotene. The variation between human and maize, which are similar in genome size, could to some extent relate to the different technical approaches applied in the two studies (DAPI staining versus FISH), since it has been noted that the FISH procedure maintains overall size and shape of the target region but may blur the fine structure of chromatin to some extent (Robinett et al., 1996). Furthermore, it cannot be excluded that we might have missed an equivalent stage to maize prezygotene, due to its brevity. The shortage of properly preserved human testis material prevented further investigations in this direction.

It has been assumed that chromosome condensation during leptotene might drive homologue alignment (Kleckner et al., 1991; Cook, 1997). Since chromosome condensation should lead to reduced volumes and surface area, the data obtained from three-dimensional analysis of chromosome morphology in human and maize meiosis (Dawe et al., 1994) are difficult to align with such a mechanism. Furthermore, it appears that the results of the present and other 3-D studies on meiotic chromosome behavior are difficult to compare with the data obtained in wild-type and mutant strains of budding yeast, since these have been performed using detergent-spread meiocyte nuclei (e.g. Scherthan et al., 1992; Loidl et al., 1994; Weiner and Kleckner, 1994; Rockmill et al., 1995).

### Chromosomes are compacted at pachytene

Pachytene chromosomes are organized in chromatin loops, which are attached at their base to meiotic chromosome cores in a genome- and a species- and locus-specific manner (Moens and Pearlman, 1988; Loidl et al., 1995; Heng et al., 1996). Human male pachytene chromosomes display a slightly reduced chromosome core length as compared to zygotene ones (Rasmussen and Holm, 1978). The present analysis revealed a decrease in volume and surface area, which indicate that an overall chromatin compaction occurs during pachytene. The reduction of surface area most likely results from the loss of the area forming the pairing interface from the overall chromosome territory surface. Larger roundness factor estimates obtained at this stage indicate that the territories occupied by the bivalents are more compacted and may have obtained a smoother surface. The condensation of pachytene chromosomes could contribute to chromosome movements leading to the dispersion of telomeres from the cluster site, where they were aggregated during the bouquet stage (e.g. Moens, 1974; Scherthan et al., 1996; Bass et al., 1997).

Volumes of pericentromeric pachytene signals were threefold increased over leptotene signals. While the twofold increase over zygotene values is the consequence of the pairing of homologous pericentromeres, the threefold volume increase over leptotene values suggests that the compaction of satellite DNA is relaxed at pachytene. This agrees with earlier observations, according to which heterochromatin is underrepresented in the SC (Stack, 1984).

We thank J. Loidl for constructive comments on an earlier draft of this manuscript, Hank W. Bass for communication of data prior to publication and J. Trent for providing arm paint probes. This study was supported by a grant from the Deutsche Forschungsgemeinschaft (Sche 350/8-1). T. C. and R. E. were supported by the German Human Genome Project (01 KW 9621/5).

## REFERENCES

**Adler, I. D.** (1996). Comparison of the duration of spermatogenesis between male rodents and humans. *Mutat. Res.* **352**, 169-172.

**Ambros, P. F. and Sumner, A. T.** (1987). Correlation of pachytene chromomeres and metaphase bands of human chromosomes and distinctive properties of telomeric regions. *Cytogenet. Cell Genet.* **44**, 223-228.

**Anderson, L. K., Offenberg, H. H., Verkuilen, W. M. H. C. and Heyting, C.** (1997). RecA-like proteins are components of early meiotic nodules in Lilly. *Proc. Nat. Acad. Sci. USA* **94**, 6868-6873.

**Aragón-Alcaide, L., Reader, S., Beven, A., Shaw, P., Miller, T. and Moore, G.** (1997). Association of homologous chromosomes during floral development. *Curr. Biol.* **7**, 905-908.

**Armstrong, S. J., Kirkham, A. J. and Hultén, M. A. J.** (1994). XY chromosome behavior in the germ-line of the human male: a FISH analysis

of spatial orientation, chromatin condensation and pairing. *Chromosome Res.* **2,** 445-452.

**Ashley, T., Plug, A. W., Xu, J., Solari, A. J., Reddy, G., Golub, E. I. and Ward, D. C.** (1995). Dynamic changes in Rad51 distribution on chromatin during meiosis in male and female vertebrates. *Chromosoma* **104**, 19-28.

**Baker, S. M., Bronne, C. E., Zhang, L., Plug, A. W., Robatzek, M., Warren, G., Elliott, E. A., Yu, J., Ashley, T., Arnheim, N., Flavell, R. A. and Liskay, R. M.** (1995). Male mice defective in the DNA mismatch repair gene PMS2 exhibit abnormal chromosome synapsis in meiosis. *Cell* **82**, 309-319.

**Barlow, A. L. and Hultén, M. A.** (1996). Combined immunocytogenetic and molecular cytogenetic analysis of meiosis I human spermatocytes. *Chromosome Res.* **4**, 562-573.

**Barlow, A. L., Benson, F. E., West, S. C. and Hultén, M. A.** (1997). Distribution of the Rad51 recombinase in human and mouse spermatocytes. *EMBO J.* **16**, 5207-5215

**Bascom-Slack, C. A. and Dawson, D. S.** (1997). The yeast motor protein, *Kar3p*, is essential for meiosis I. *J. Cell Biol.* **139**, 459-467

**Bass, H. W., Marshall, W. F., Sedat, J. W., Agard, D. A. and Cande, W. Z.** (1997). Telomeres cluster de novo before the initiation of synapsis: athree-dimensional spatial analysis of telomere positions before and duringmeiotic prophase. *J. Cell Biol.* **137**, 5-18.

**Baumann, P., Benson, F. E. and West, S. C.** (1996). Human Rad51 protein promotes ATP-dependent homologous pairing and strand transfer reactions in vitro. *Cell* **87**, 757-766.

**Bishop D. K.** (1994). RecA homologs Dmc1 and Rad51 interact to form multiple nuclear complexes prior to meiotic chromosome synapsis. *Cell* **79,** 1081-1092.

**Boiko, M.** (1983). Human meiosis VIII. Chromosome pairing and formation of the synaptonemal complex in oocytes. *Carlsberg Res. Commun.* **48**, 457-483.

**Carpenter, A. T.** (1987). Gene conversion, recombination nodules and initiation of meiotic synapsis. *BioEssays* **6**, 232-236.

**Cheng, E. Y. and Gartler, S. M.** (1994). A fluorescent in situ hybridization analysis of X chromosome pairing in human female meiosis. *Hum. Genet.* **94**, 389-394.

**Chikashige, Y., Ding, D. Q., Funabiki, H., Haraguchi, T., Mashiko, S., Yanagida, M. and Hiraoka, Y.** (1994). Telomere-led premeiotic chromosome movement in fission yeast. *Science* **264**, 270-273.

**Chikashige, Y., Ding, D. Q., Imai, Y., Yamamoto, M., Haraguchi, T. and Hiraoka, Y.** (1997). Meiotic nuclear reorganization: switching the position of centromeres and telomeres in the fission yeast *Schizosaccharomyces pombe*. *EMBO J.* **16**, 193-202.

**Comings, D. E.** (1980). Arrangement of chromatin in the nucleus. *Hum. Genet.* **53**, 131-143

**Cook, P. R.** (1997). The transcriptional basis of chromosome pairing. *J. Cell Sci.* **110**, 1033-1040.

**Craig, J. M. and Bickmore, W. A.** (1994). The distribution of CpG islands in mammalian chromosomes. *Nat. Genet.* **7**, 376-382

**Cremer, T., Kurz, A., Zirbel, R., Rinke, B., Dietzel, S., Schröck, E., Speicher, M. R., Ried, T., Matthieu, U., Jauch, A., Emmerich, P., Scherthan, H., Cremer, C. and Lichter, P.** (1993). Role of chromosome territories in the functional compartmentalization of the cell nucleus. *Cold Spring Harbor Symp. Quant. Biol.* **58**, 777-792.

**Dawe, K. R., Sedat, J. W., Agard, D. A. and Cande, Z. W.** (1994). Meiotic chromosome pairing in maize is associated with a novel chromatin organization. *Cell* **76**, 901-912.

**Dernburg, A. F., Sedat, J. W. and Hawley, R. S.** (1996). Direct evidence of a role for heterochromatin in meiotic chromosome segregation. *Cell* **86**, 135-146.

**Dernburg, A. F., Sedat, J. W., Cande, W. Z. and Bass, H. W.** (1995). The cytology of telomeres. In *Telomeres* (ed. E. H. Blackburn and C. W. Greider), pp. 295-338. CSH Press, Cold Spring Harbor Monograph Series.

**Dietrich, A. J. J. and de Boer, P.** (1983). A sequential analysis of the development of the synaptonemal complex in spermatocytes of the mouse by electron microscopy using hydroxyurea and agar filtration. *Genetica* **61**, 119-129.

**Dietzel, S., Jauch, A., Kienle, D., Qu, G., Holtgreve-Grez, H., Eils, R., Münkel, C., Bittner, M., Meltzer, P. S., Trend, J. M. and Cremer, T.** (1998). Separate and variably shaped chromosome arm domains are disclosed by chromosome arm painting in human cell nuclei. *Chromosome Res.* **6**, 25-33.

**Ding, D. Q., Chikashige, Y., Haraguchi, T. and Hiraoka, Y.** (1998). Oscillatory nuclear movement in fission yeast meiotic prophase is driven by astral microtubules, as revealed by continuous observation of chromosomes and microtubules in living cells. *J. Cell Sci.* **111**, 701-712.

**Eils, R., Bertin, E., Saracoglu, K., Rinke, B., Schröck, E., Parazza, F., Usson, Y., Robert-Nicoud, M., Stelzer E. H. K., Chassery, J.-M., Cremer, T. and Cremer, C.** (1995a). Application of laser confocal microscopy and 3D-Voronoi diagrams for volume and surface estimates of interphase chromosomes. *J. Microscopy* **177,** 150-161.

**Eils, R., Saracoglu K., Münkel, C., Imhoff, J., Sätzler, K., Bertin, E., Dietzel, S., Schröck, E., Ried, T. Cremer, T. and Cremer, C.** (1995b). Three-dimensional imaging approaches and Monte Carlo simulations: development of tools to study the morphology and distribution of chromosome territories and subchromosomal targets in human cell nuclei. *Zoological Studies* **34**, Supplement I, 7-10.

**Eils, R., Dietzel, S., Bertin, E., Schröck, E., Speicher, M. R., Ried, T., Robert-Nicoud, M., Cremer, C. and Cremer, T.** (1996). Three-dimensional reconstruction of painted human interphase chromosomes: active and inactive X-chromosome territories have similar volumes but differ in shape and surface structure. *J. Cell Biol.* **135**, 1427-1440.

**Ferguson, M. and Ward, D. C.** (1992). Cell cycle dependent chromosomal movement in pre-mitotic human T-lymphocyte nuclei. *Chromosoma* **101**, 557-565.

**Ferreira, J., Paolella, G., Ramos, C. and Lamond, A. I.** (1997). Spatial organization of large-scale chromatin domains in the nucleus: a magnified view of single chromosome territories. *J. Cell Biol.* **139**, 1597-1610.

**Funabiki, H., Hagan, I., Uzawa, S. and Yanagida, M.** (1993). Cell cycle-dependent specific positioning and clustering of centromeres and telomeres in fission yeast. *J. Cell Biol.* **121**, 961-976

**Fussell, C. P.** (1987). The Rabl orientation: A prelude to synapsis. In *Meiosis* (ed. P. B. Moens), pp. 275-299. Academic Press, Orlando.

**Goldman, A. S. and Lichten, M.** (1996). The efficiency of meiotic recombination between dispersed sequences in *Saccharomyces cerevisiae* depends upon their chromosomal location. *Genetics* **144**, 43-55.

**Guan, X. Y., Zhang, H., Bittner, M., Jiang, Y., Meltzer, P. and Trent, J.** (1996). Chromosome arm painting probes. *Nat. Genet.* **12**, 10-11.

**Haber, J. E., Leung, W. Y., Borts, R. H. and Lichten, M.** (1991). The frequency of meiotic recombination in yeast is independent of the number and position of homologous donor sequences: implications for chromosome pairing. *Proc. Nat. Acad. Sci. USA* **88,** 1120-1124.

**Hawley, R. S. and Arbel, T.** (1993). Yeast genetics and the fall of the classical view of meiosis. *Cell* **72**, 301-303.

**Heng, H. H., Chamberlain, J. W., Shi, X. M., Spyropoulos, B., Tsui, L. C. and Moens, P. B.** (1996). Regulation of meiotic chromatin loop size by chromosomal position. *Proc. Nat. Acad. Sci. USA* **93**, 2795-2800.

**Heyting, C.** (1996). Synaptonemal complexes: structure and function. *Curr. Opin. Cell Biol.* **8**, 389-396

**Hiraoka, Y., Dernburg, A. F., Parmerlee, S. J., Rykowski, M. C., Agard, D. A. and Sedat, J. W.** (1993). The onset of homologous chromosome pairing during *Drosophila melanogaster* embryogenesis. *J. Cell Biol.* **120**, 591-600.

**Jackson, D. A. and Cook, P. R. (**1995). The structural basis of nuclear function. *Int. Rev. Cytol.* **162,** 125-149.

**Jin, Q.-W., Trelles-Sticken, E., Scherthan, H. and Loidl, J.** (1998). Yeast nuclei display prominent centromere clustering which is reduced in non-dividing cells and in meiotic prophase. *J. Cell Biol.* **141**, 21-29.

**Jinks-Robertson, S. and Petes, T. D.** (1985). High-frequency meiotic gene conversion between repeated genes on non-homologous chromosomes. *Proc. Nat. Acad. Sci. USA* **82**, 3350-3354.

**John, B.** (1990). *Meiosis*. Cambridge University Press: Cambridge, New York, Sidney.

**Karpen, G. H., Le, M. H. and Le, H.** (1996). Centric heterochromatin and the efficiency of achiasmate disjunction in Drosophila female meiosis. *Science* **273**, 118-122.

**Kleckner, N.** (1996). Meiosis: how could it work? *Proc. Nat. Acad. Sci. USA* **93**, 8167-8174.

**Kleckner, N., Padmore, R. and Bishop, D. K.** (1991). Meiotic chromosome metabolism: one view. *Cold Spring Harbor Symp. Quant. Biol.* **56**, 729-743.

**Kleckner, N. and Weiner, B.** (1993). Potential advantages of unstable interactions for pairing in meiotic, somatic, and premeiotic cells. *Cold Spring Harbor Symp. Quant. Biol.* **58**, 553-565.

**Kohli, J. (**1994). Telomeres lead chromosome movement. *Curr. Biol.* **4**, 724-727.

**Kurz, A., Lampel, S., Nickolenko, J. E., Bradl, J., Benner, A., Zirbel, R. M., Cremer, T. and Lichter, P.** (1996). Active and inactive genes localize

preferentially in the periphery of chromosome territories. *J. Cell Biol.* **135**, 1195-1205.

**Loidl, J.** (1990). The initiation of meiotic chromosome pairing: the cytological view. *Genome* **33**, 759-778.

**Loidl, J. and Länger, H.** (1993). Evaluation of models of homologue search with respect to their efficiency on meiotic pairing. *Heredity* **71**, 342-351

**Loidl, J., Klein, F. and Scherthan, H.** (1994). Homologous pairing is reduced but not abolished in asynaptic mutants of yeast. *J. Cell Biol*. **125**, 1191-1200.

**Loidl, J., H., Scherthan, J. T., Dunnen, D. and Klein, F.** (1995). Morphology of a human-derived YAC in Yeast meiosis. *Chromosoma* **104**, 183-188.

**Luciani, J. M., Guichaoua, M. R., Cau, P., Devictor, B. and Salagnon, N.** (1988). Differential elongation of autosomal pachytene bivalents related to their DNA content in human spermatocytes. *Chromosoma* **97**, 19-25.

**Maguire, M. P.** (1972). Role of heterochromatin in homologous chromosome pairing: evaluation of evidence. *Science* **176**, 543-544.

**Marshall, W. F., Straight, A., Marko, J. F., Swedlow, J., Dernburg, A., Belmont, A., Murray, A. W., Agard, D. A. and Sedat, J. W.** (1997). Interphase chromosomes undergo constrained diffusional motion in living cells. *Curr. Biol.* **7**, 930-939.

**Moens, P. B.** (1974). Quantitative electron microscopy of chromosome organization at meiotic prophase. *Cold Spring Harbor Symp. Quant. Biol.*, **38**, 99-107.

**Moens, P. B. and Pearlman, R. E.** (1988). Chromatin organization at meiosis. *BioEssays* **9**, 151-153.

**Moses, M. J.** (1968). Synaptinemal Complex. *Ann. Rev. Genetics* **2**, 363-412.

**Murti, J. R., Bumbulis, M. and Schimenti, J. C.** (1994). Gene conversion between unlinked sequences in the germline of mice. *Genetics* **137**, 837-843.

**Nagele, R., Freeman, T., McMorrow, L. and Lee, H.-Y.** (1995). Precise spatial positioning of chromosomes during prometaphase: evidence for chromosomal order. *Science* **270**, 1831-1835.

**Oud, J. L. and Reutlinger, A. H. H.** (1981). Chromosome behaviour during early meiotic prophase of mouse spermatocytes. *Chromosoma* **83**, 395-407.

**Parvinnen, M. and Söderström, K.-O.** (1976). Chromosome rotation and formation of synapsis. *Nature* **260**, 534-535.

**Plug, A. W., Peters, A. H., Keegan, K. S., Hoekstra, M. F., de Boer, P. and Ashley, T.** (1998). Changes in protein composition of meiotic nodules during mammalian meiosis. *J. Cell Sci.* **111**, 413-423.

**Quien, N. and Müller, W.** (1992). Gothic Vaults and Transputers. IEEE *Computer Graphics & Applications* **12**, 12-13.

**Radman, M. and Wagner, R.** (1993). Mismatch recognition in chromosomal interactions and speciation. *Chromosoma* **102**, 369-373.

**Rasmussen, S. W. and Holm, P. B.** (1978). Human Meiosis II. Chromosome pairing and recombination nodules in human spermatocytes. *Carlsberg Res. Com.* **43**, 275-327.

**Rasmussen, S. W. and Holm, P. B.** (1980). Mechanics of Meiosis. *Hereditas* **93**, 187-216.

**Rhoades, M. M.** (1961). Meioses. In *The Cell: Biochemistry, Physiology and Morphology*, Vol. 3: Meiosis and Mitosis (ed. J. Brachet and A. E. Mirsky), pp. 1-75. Academic Press, New York.

**Robinett, C. C., Straight, A., Li, G., Willhelm, C., Sudlow, G., Murray, A. and Belmont, A. S.** (1996). In vivo localization of DNA sequences and visualization of large-scale chromatin organization using lac operator/repressor recognition. *J. Cell Biol.* **135**, 1685-1700.

**Rockmill, B., Sym, M., Scherthan, H. and Roeder, G. S.** (1995). Two RecA homologs facilitate meiotic chromosome synapsis by establishing connections between homologous chromosomes. *Genes Dev.* **9**, 2684-2695.

**Roeder, G. S.** (1995). Sex and the single cell: meiosis in yeast. *Proc. Nat. Acad. Sci. USA* **92**, 10450-10456.

**Roeder, G. S.** (1997). Meiotic chromosomes: it takes two to tango. *Genes Dev.* **11**, 2600-2621.

**Sachs, R. K., van den Engh, G., Trask, B., Yokota, H. and Hearst, J. E.** (1995). A random-walk/giant-loop model for interphase chromosomes. *Proc. Nat. Acad. Sci. USA* **92**, 2710-2714.

**Salonen, K., Paranko, J. and Parvinen, M.** (1982). A colcemid sensitive mechanism involved in regulation of chromosome movements during meiotic pairing. *Chromosoma* **85**, 611-618.

**Scherthan, H., Loidl, J., Schuster, T. and Schweizer, D.** (1992). Meiotic chromosome condensation and pairing in *Saccharomyces cerevisiae* studied by chromosome painting. *Chromosoma* **101**, 590-595.

**Scherthan, H. and Cremer, T.** (1994). Methodology of non isotopic in situ-hybridization in embedded tissue sections. In *Methods in Molecular Genetics* **5** (ed. K. W. Adolph), pp. 223-238. Academic Press, San Diego.

**Scherthan, H., Bähler, J. and Kohli, J.** (1994). Dynamics of chromosome organization and pairing during meiotic prophase of fission yest. *J. Cell Biol.* **127**, 273-285.

**Scherthan, H., Weich, S., Schwegler, H., Heyting, C., Härle, M. and Cremer, T.** (1996). Centromere and telomere movements during early meiotic prophase of mouse and man are associated with the onset of chromosome pairing. *J. Cell Biol.* **134**, 1109-1125.

**Scherthan, H.** (1997). Chromosome behavior in earliest meiotic prophase. In *Chromosomes Today*, Vol. 12 (ed. H. Gill, J. S. Parker and M. Puertas), pp. 217-248. Chapman and Hall, London.

**Schmekel, K. and Daneholt, B.** (1995). The central region of the synaptonemal complex revealed in three dimensions. *Trends Cell Biol.* **5**, 239-242.

**Schulze, W. and Rehder, U.** (1984) Organization and morphogenesis of the human seminiferous epithelium. *Cell Tissue Res.* **237**:395-407

**Schwarzacher, T.** (1997). Three stages of meiotic homologous chromosome pairing in wheat:cognition, alignment and synapsis. *Sexual Plant Reprod.* **10**, 324-331.

**Selig, S., Okumura, K., Ward, D. C. and Cedar, H.** (1992). Delineation of replication time zones by fluorescence in situ hybridization. *EMBO J.* **11**, 1217-1225.

**Smith, A. and Benavente, R.** (1995). An $M_r$ 51,000 protein of mammalian spermatogenic cells that is common to the whole XY body and centromeric heterochromatin of autosomes. *Chromosoma* **103**, 591-596.

**Smithies, O. and Powers, P. A.** (1986). Gene conversions and their relation to to homologous chromosome pairing. *Phil. Trans. R. Soc. Lond. B* **312**, 291-302

**Stack, S. M.** (1984). Heterochromatin, the synaptonemal complex and crossing over. *J. Cell Sci.* **71**, 159-176.

**Svoboda, A., Bähler, J. and Kohli, J.** (1995). Microtubule-driven nuclear movements and linear elements as meiosis-specific characteristics of the fission yeasts *Schizosaccharomyces versatilis* and *Schizosaccharomyces pombe*. *Chromosoma* **104**, 203-214

**Terasawa, M., Shinohara, A., Hotta, Y., Ogawa, H. and Ogawa, T.** (1995). Localization of RecA-like recombination proteins on chromosomes of the lily at various meiotic stages. *Genes Dev.* **9**, 925-934

**Vocero-Akbani, A., Helms, C., Wang, J. C., Sanjurjo, F. J., Korte-Sarfaty, J., Veile, R. A., Liu, L., Jauch, A., Burgess, A. K., Hing, A. V., Holt, M. S., Ramachandra, S., Whelan, A. J., Anker, R., Ahrent, L., Chen, M., Gavin, M. R., Iannantuoni, K., Morton, S. M., Pandit, S. D., Read, C. M., Steinbrueck, T., Warlick, C., Smoller, D. A. and Donis-Keller, H.** (1996). Mapping human telomere regions with YAC and P1 clones: Chromosome specific markers for 27 telomeres including 149 STSs and 24 polymorphisms for 14 proterminal regions. *Genomics* **36**, 492-506.

**von Wettstein, D., Rasmussen, S. W. and Holm, P. B.** (1984). The synaptonemal complex in genetic segregation. *Annu. Rev. Genet.* **18**, 331-413.

**Vourc'h, C., Taruscio, D. Boyle, A. L. and Ward, D. C.** (1993). Cell cycle-dependent distribution of telomeres, centromeres and chromosome-specific subsatellite domains in the interphase nucleus of mouse lymphocytes. *Exp. Cell Res.* **205**, 142-151.

**Wandall, A. and Svendsen, A.** (1985). Transition from somatic to meiotic pairing and progressional changes of the synaptonemal complex. *Chromosoma* **92**, 254-264.

**Waye, J. S. and Willard, H. F.** (1989). Chromosome specificity of satellite DNAs: short- and long-range organization of a diverged dimeric subset of human alpha satellite from chromosome 3. *Chromosoma* **97**, 475-480.

**Weiner, B. and Kleckner, N.** (1994). Chromosome pairing via multiple interstitial interactions before and during meiosis in yeast. *Cell* **77**, 977-991.

**Wu, T. C. and Lichten, M.** (1994). Meiosis-induced double-strand break sites determined by yeast chromatin structure. *Science* **263**, 515-518

**Yokota, H., van den Engh, G., Hearst, J. E., Sachs, R. K. and Trask, B. J.** (1995). Evidence for the organization of chromatin in megabase pair-sized loops arranged along a random walk path in the human $G_0/G_1$ interphase nucleus. *J. Cell Biol.* **130**, 1239-1249:

**Young, I. T.** (1977). Proof without prejudice: Use of the Kolmogorov-Smirnov test for the analysis of histograms from flow systems and other sources. *J. Histochem. Cytochem.* **25**, 935-941.

**Zalensky, A. O., Tomilin, N. V., Zalenskaya, I. A., Teplitz, R. L. and Bradbury, E. M.** (1997). Telomere-telomere interactions and candidate telomere binding protein(s) in mammalian sperm cells. *Exp. Cell Res.* **232**, 29-41.

**Zink, D., Cremer, T., Saffrich, R., Fischer, R., Trendelenburg, M. F., Ansorge, W. and Stelzer, E. H.** (1998). Structure and dynamics of human interphase chromosome territories in vivo. *Hum. Genet.* **102,** 241-251.